ROYAL SOCIETY OF CHEMISTRY

PAPER

Check for updates

Biomass-derived activated carbon from *Scolymus hispanicus*: activation strategy and adsorption mechanism of hydroxychloroquine

Amel Hamadi, [ID] *[a] Imene Hammoudi,[a] Fayçal Finnouche,[a] Hiba Kais,[a] Nacera Yeddou-Mezenner[a] and Zaki Nekkaa[b]

Biosorption offers a sustainable approach for the removal of pharmaceutical contaminants from wastewater. This study reports, for the first time, the use of activated carbon derived from *Scolymus hispanicus* biomass as a low-cost, eco-friendly adsorbent for the removal of hydroxychloroquine sulfate (HCQ) from aqueous solutions. Adsorption performance was evaluated through equilibrium and kinetic studies, with data analyzed using Langmuir and Freundlich isotherm models, a pseudo-second-order kinetic model, and intraparticle diffusion analysis to elucidate the underlying adsorption mechanism. The biosorbent exhibited a maximum adsorption capacity of 23.17 mg g^{-1} under the investigated conditions. Thermodynamic parameters ($\Delta G°$, $\Delta H°$, and $\Delta S°$) were independently determined, revealing that the adsorption process is spontaneous and endothermic, as inferred from negative $\Delta G°$ and positive $\Delta H°$ values, rather than from adsorption capacity alone. The integrated analysis of isotherm, kinetic, and thermodynamic results provides a comprehensive mechanistic interpretation. This work highlights the novelty of using *Scolymus hispanicus* as a sustainable precursor and demonstrates its potential as a cost-effective and environmentally friendly alternative to conventional activated carbons for pharmaceutical wastewater treatment.

1 Introduction

The contamination of the environment by persistent organic compounds, especially pharmaceutical residues, poses a significant threat to both human health and ecosystems. These micropollutants, although found in extremely low concentrations, primarily stem from hospital, industrial, and household sources.[1] Their durability in aquatic environments, resistance to standard treatment methods, and potential toxicity have become matters of growing concern.[2] Pharmaceutical compounds frequently identified in aquatic environments include anti-inflammatory agents, antibiotics, hormones, beta-blockers, and antimalarials, such as hydroxychloroquine (HCQ).[3] HCQ, widely used in the treatment of diseases like rheumatoid arthritis and systemic lupus erythematosus,[4–8] is commonly detected in discharges from the pharmaceutical industry, hospital effluents, wastewater treatment facilities, laboratory waste, and excreta from both humans and animals.[9]

The widespread discharge of hydroxychloroquine (HCQ) into aquatic environments represents a critical emerging contaminant, capable of accelerating antimicrobial resistance in pathogenic bacteria and inducing ecotoxicological effects in aquatic organisms, with potential repercussions for human health. As concentrations of such pharmaceutical residues continue to rise in municipal wastewater and industrial effluents, there is an urgent need to develop and implement efficient and sustainable removal strategies. Advancing such treatment approaches is essential not only for safeguarding water quality but also for mitigating the broader public health risks associated with the proliferation of drug-resistant microorganisms.

Several physicochemical approaches have been developed to tackle this emerging form of pollution, with adsorption being particularly favored for its effectiveness, straightforward application, and affordability.[10–12] Adsorption has emerged as a promising approach for the removal of various emerging organic and inorganic pollutants, such as heavy metals,[13] toxic gases,[14] synthetic dyes,[15] and pharmaceutical compounds.[16,17] However, adsorption efficiency largely depends on the characteristics of the adsorbent material used.[18] Consequently, the use of natural or plant-based adsorbents contributes to environmental sustainability by reducing ecological impact and promoting renewable resource utilization.[19]

In this study, *Scolymus hispanicus*, an abundant Mediterranean plant, was investigated for the first time as a sustainable and low-cost precursor for the production of activated carbon (SHAC). The primary objective was to evaluate the effectiveness

[a]Laboratory of Engineering of Reaction, Department of Environmental Engineering, Faculty of Mechanical Engineering and Process Engineering, University of Science and Technology Haouari Boumediene, Algiers, Algeria

[b]National Office of Geological and Mining Research (ORGM), Boumresdes, Algiers, Algeria

of SHAC as an adsorbent for the removal of hydroxychloroquine (HCQ), an emerging pharmaceutical contaminant, from aqueous solutions. To achieve this, the adsorbent was synthesized using both physical and chemical activation techniques and subsequently characterized to elucidate its textural properties and surface chemistry. A comprehensive examination of the adsorption process was conducted, including systematic studies of operational parameters, kinetic modeling, equilibrium isotherms, and thermodynamic behavior. These analyses provide critical insights into the mechanisms governing HCQ uptake and demonstrate the potential of *S. hispanicus*-derived activated carbon as an eco-friendly alternative to conventional adsorbents. Recent research[20] has highlighted the growing interest in biomass-derived activated carbons for removing pharmaceutical pollutants from wastewater, with studies reporting high adsorption capacities and favorable kinetics when using agricultural waste.

2 Materials and methods

2.1 Solution preparation

Hydroxychloroquine sulfate (HCQ) is a water-soluble pharmaceutical compound characterized by two prominent absorption peaks at 333 nm and 343 nm. A stock solution with a concentration of 200 mg L^{-1} was prepared by accurately dissolving a measured amount of anhydrous HCQ in deionized water. The molecular structure and key physicochemical properties of HCQ are presented in Table 1.

2.2 Preparation of *Scolymus hispanicus* activated carbon

The activated carbon used in this study was derived from *Scolymus hispanicus*, an agricultural waste material collected in the Ain Defla region of Algeria during the month of August. The raw material was first thoroughly washed several times with tap water, followed by distilled water, to eliminate dust and surface impurities. Washing continued until the rinse water appeared clear. Afterward, the samples were air-dried at room temperature and subsequently dried in an oven at 105 °C for 24 hours. The dried material was then ground and sieved to obtain a powder with a particle size ranging from 1 to 1.25 mm.

In this research, *Scolymus hispanicus* was first dried and then mixed with zinc chloride (ZnCl$_2$) in a 1 : 1 weight ratio.[21] Water was added to facilitate the formation of a homogeneous paste,[22] which was then subjected to carbonization *via* physical activation in a furnace at 873 K for 4 hours. Following activation, the material was repeatedly washed with distilled water to eliminate

residual activating agents, then dried at 363 K for 24 hours, and stored under appropriate conditions, as depicted in Fig. 1.

The surface morphology and structural features of the activated carbon were characterized using Scanning Electron Microscopy (SEM, JEOL JSM-6830) and BET surface area analysis, conducted with a Micromeritics ASAP 2420 analyzer employing liquid nitrogen at −196 °C.

2.3 Batch adsorption experiments

Adsorption experiments were performed in batch mode by introducing 0.5 g of activated carbon *Scolymus hispanicus* (SHAC) into 1 liter of a synthetic HCQ solution at a concentration of 10 mg L^{-1}. The solution was agitated at 400 rpm for predetermined time intervals. At specified times, samples were withdrawn and filtered using a syringe filter. The filtrates were analyzed with an OPTIZEN 2120 UV-vis spectrophotometer at a wavelength of 333 nm ($\lambda = 333$ nm).[23]

The HCQ removal rate was calculated using the following equation:

$$\% \text{ Removal} = \frac{C_0 - C_t}{C_0} \times 100 \tag{1}$$

where R% is the HCQ percentage removal, C_0 (mg L^{-1}) is the initial HCQ concentrations in the solution, C_t (mg L^{-1}) is the HCQ concentration at time t.

The amount of adsorbed HCQ per unit weight of SHAC, q_t (mg g^{-1}), was determined using the following equation:

$$q_t = \frac{C_0 - C_t}{m} \times V \tag{2}$$

where q_t (mg g^{-1}) is the amounts of adsorbed HCQ after time t (min), C_0 (mg L^{-1}), is the initial HCQ concentrations in the aqueous solution, C_t (mg L^{-1}) is the HCQ concentration in the aqueous solution at time t (min), V (L) is the volume of the solution, and m is the SHAC weight, g.
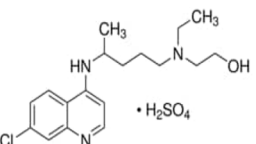
3 Results and discussion

3.1 Characterization of SHAC

3.1.1 Isoelectric point pH. The point of zero charge (pHpzc) is a critical parameter in adsorption studies, as it indicates the pH at which the adsorbent surface carries a neutral net charge, where the number of positive and negative surface charges is equal.

In this study, the pHpzc was determined according to the method described by Giles.[24] A series of closed flasks, each

Table 1 Chemical structure and geometric properties of HCQ

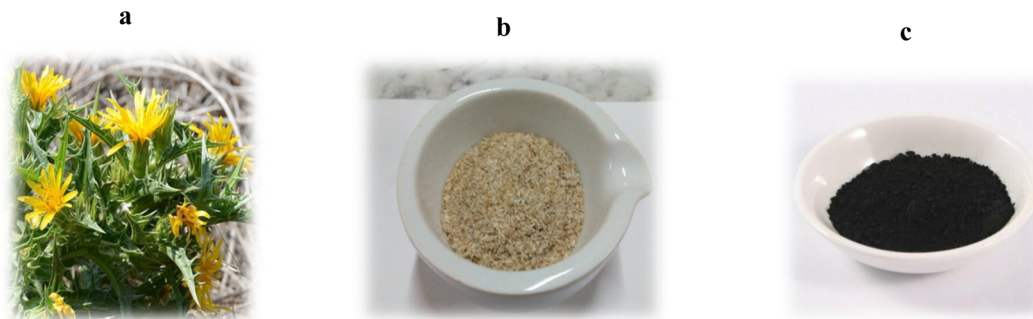| Structure	Molecul formula	Chemical name	MW (g mol^{-1})	$\lambda_{\max}$ (nm)	Purty	Storage	Stability
	$C_{18}H_{26}ClN_3O \cdot H_2SO_4$	2-[[4-[(7-Chloro-4-quinolyl)amino]pentyl]ethylamino] ethanol sulfate[11]	434	333	≥95%	20 °C	≥2 years

Fig. 1 (a) *Scolymus hispanicus* plant, (b) *Scolymus hispanicus* powder, and (c) *Scolymus hispanicus* activated carbon.

containing 50 mL of a 0.01 M KNO_3 solution, was prepared. The initial pH of each solution was adjusted within the range of 2 to 11 using 0.1 N NaOH or HCl. Afterward, 0.1 g of the adsorbent was added to each flask. The mixtures were stirred for 48 hours, after which the final pH was measured. The pHpzc was identified as the pH value at which the difference between the initial and final pH (ΔpH) equals zero, as observed from the intersection point on the curve plotting final pH against initial pH (Fig. 2).

3.1.2 Specific surface area analysis by BET. The Brunauer–Emmett–Teller (BET) method is commonly employed to assess the textural properties of solid materials, such as specific surface area, pore volume, and average pore diameter. This technique involves the physical adsorption of a gas, typically nitrogen 77, onto the material's surface. The adsorption isotherm obtained is then interpreted using the BET model to calculate the specific surface area, while the pore size distribution is determined *via* the BJH (Barrett–Joyner–Halenda) method.

In this study, the analyses were conducted using a Micromeritics ASAP 2420 surface area and porosity analyzer under liquid nitrogen conditions (−196 °C).

Fig. 3 illustrates that the isotherm corresponds to a type IV profile according to the IUPAC classification,[25] which is characteristic of mesoporous materials. At low relative pressures, nitrogen adsorption is relatively weak, followed by a progressive

increase in the adsorbed volume. A well-defined hysteresis loop is observed, indicating the presence of mesopores and suggesting that nitrogen is retained within the pores during desorption, a common behavior in materials with complex porous networks.

The specific surface area, determined using the Brunauer–Emmett–Teller (BET) method (eqn (3)), is 258.13 m^2 g^{-1}, reflecting a good adsorption capacity. The total pore volume, estimated from the amount of nitrogen adsorbed at high relative pressure, is 0.202 cm^3 g^{-1}. Using the Barrett–Joyner–Halenda (BJH) method applied to the desorption branch of the isotherm, the average pore diameter is found to be approximately 37 Å, confirming the predominance of mesoporosity. All proprieties are listed in Table 1.

These results indicate that the SHAC exhibits well-developed porosity, making it a promising candidate for the adsorption of organic molecules in solution, such as hydroxychloroquine sulfate.

$$S_{BET} = \frac{S_T}{a} \qquad (3)$$

where S_{BET} is the BET surface area (m^2 g^{-1}), S_T is surface area total (m^2 g^{-1}), and a is the masse of adsorbent (g)

$$S_T = \frac{V_m}{V} \times N \times \sigma \qquad (4)$$

where V_m is the monolayer adsorption amount, V is the molar volume (22.414 L), N is the Avogadro number, and σ is the adsorption cross section of adsorbing species (0.162 nm^2 for N_2).

The monolayer adsorption amount is calculated from the equation of BET, represented in the following equation:

$$\frac{P}{V(P^0 - P)} = \frac{1}{C \times V_m} + \frac{C - 1}{C \times V_m} \times \frac{P}{P^0} \qquad (5)$$

where C is a constant, P is the pressure and P^0 is the saturant vapour pressure (atm).

3.1.3 Scanning electron microscope (SEM). Scanning Electron Microscopy (SEM) is a powerful imaging technique used to examine the surface morphology of solid materials at high resolution. It generates detailed images of a material's topography, offering insights into features such as shape, texture, grain size, and agglomeration.
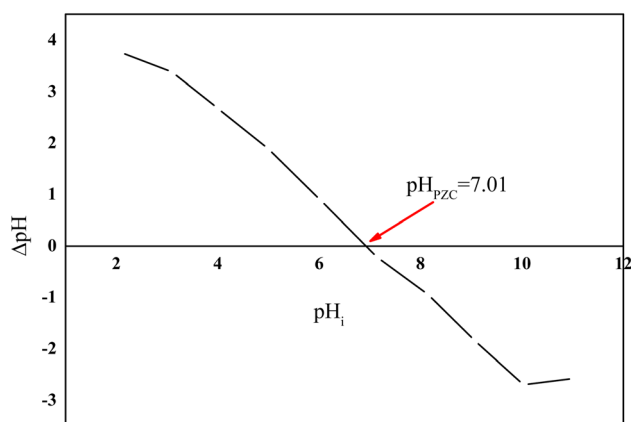

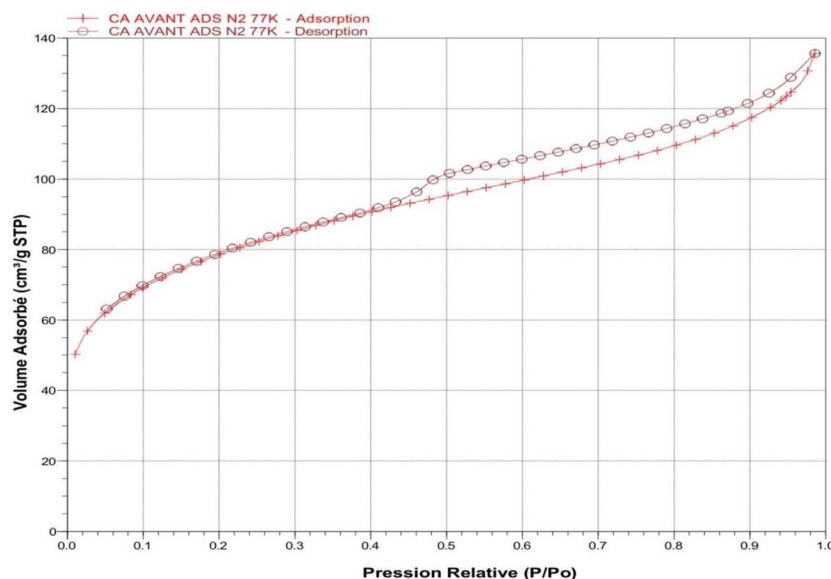
Fig. 2 Isoelectric point pH of activated carbon.

Fig. 3 Nitrogen (N_2) adsorption–desorption isotherm at 77 K on activated carbon derived from *Scolymus hispanicus* (SHAC).

In this study, the morphological characterization of the SHAC was conducted using a Philips XL30 ESEM-EDS scanning electron microscope. The SEM images revealed a highly porous surface, along with information on the particle size distribution and overall structural organization of the carbon material.

The SEM image of activated carbon before adsorption (Fig. 4a) reveals a highly irregular and rough surface, characteristic of a well-activated material. This morphology emphasizes the presence of well-developed macropores, identifiable as circular or oval shaped cavities that serve as access channels to the internal microporous network. The overall porous and fragmented structure, resulting from the physical or chemical activation processes, contributes to a high specific surface area, which is essential for efficient adsorption. Moreover, the absence of surface deposits or clogging confirms that the

material remains in its pristine state, free from interactions with contaminants. This open and accessible structure enhances the material's potential for adsorbing pollutants from aqueous media. However, after adsorption (Fig. 4b), SEM analysis reveals notable changes in the surface morphology. A partial to nearly complete coverage of the porous walls by dense, irregular deposits is observed, indicating the successful adsorption of molecules from solution.

These morphological transformations provide direct visual evidence of the interaction between SHAC and hydroxychloroquine (HCQ) molecules, confirming that the active adsorption sites have been effectively engaged.

3.1.4 Crystalline structure (XRD). X-ray Diffraction (XRD) is an analytical technique used to examine the crystalline structure of materials. When applied to activated carbon, it helps
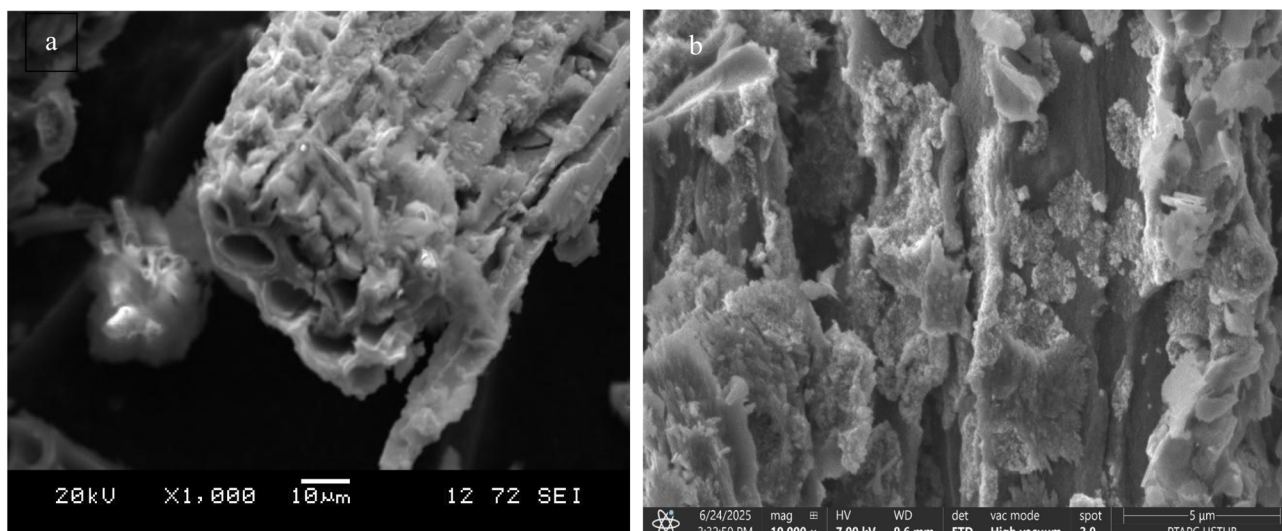

Fig. 4 SEM image of SHAC (a) before adsorption and (b) after adsorption.

determine the presence of crystalline phases, estimate crystallite size, and assess the degree of graphitization. While activated carbon is mainly amorphous, it can contain small amounts of crystalline regions, which XRD is capable of detecting. Thus, XRD analysis offers valuable structural information that complements the morphological and textural characterization of activated carbon.

The XRD analysis of activated carbon produced from *Scolymus hispanicus* shows a broad peak in the 20°–30° (2θ) range, indicating the presence of an amorphous carbon structure typical of well-carbonized biomass. However, several sharp and distinct diffraction peaks are also observed, confirming the presence of crystalline phases. These have been identified as anorthite ($CaAl_2Si_2O_8$), zincite (ZnO), simonkolleite [$Zn_5(OH)_8Cl_2 \cdot H_2O$], and anhydrite ($CaSO_4$). Such compounds may result from naturally occurring mineral content in the plant or from chemical additives used during the activation process. The detection of zinc-based phases suggests either contamination or purposeful inclusion, which may affect the material's surface functionality. Overall, the pattern reveals a mixed composition: primarily amorphous carbon, with residual crystalline mineral phases that could influence the adsorptive or catalytic properties of the activated carbon (Fig. 5).

3.2 Parametric study

3.2.1 Effect of contact time and initial concentration of HCQ. The influence of the initial HCQ concentration on the adsorption process was examined under optimal conditions.

A clear trend is observed in which increasing the initial concentration of HCQ results in a reduced removal efficiency (Fig. 6). For example, at a concentration of 5 mg L^{-1}, the removal efficiency surpasses 60% after 200 minutes, whereas at

25 mg L^{-1}, it falls below 30%. This indicates that the adsorption process is more favorable at lower concentrations.[23]

The decline in performance at higher concentrations can be explained by the slower adsorption kinetics, which are influenced by several sequential steps: (1) migration of HCQ molecules toward the surface of the adsorbent, (2) diffusion through the external (boundary) layer, and (3) intraparticle diffusion into the porous network of the activated carbon.[24] At higher concentrations, HCQ molecules have a greater tendency to aggregate, which can impede their diffusion and limit their ability to interact effectively with the available active sites on the adsorbent surface. In addition, saturation of adsorption sites and restricted accessibility to the porous surface further
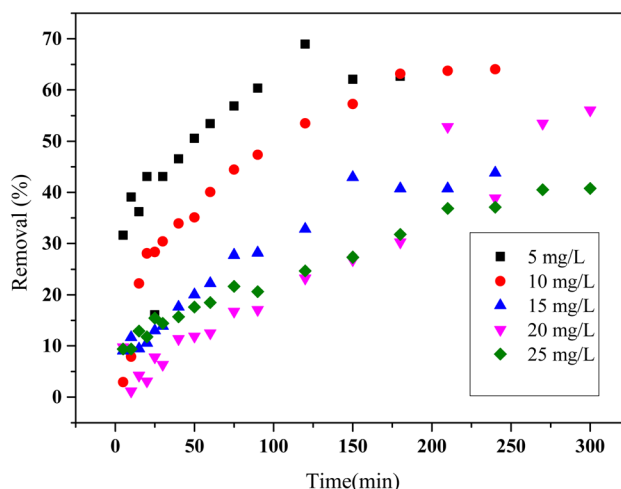

Fig. 6 Effect of initial concentration on the adsorption of HQC onto SHAC (conditions: pH = 6, 0.5 g L^{-1} of 25 °C of adsorbent dose and temperature).
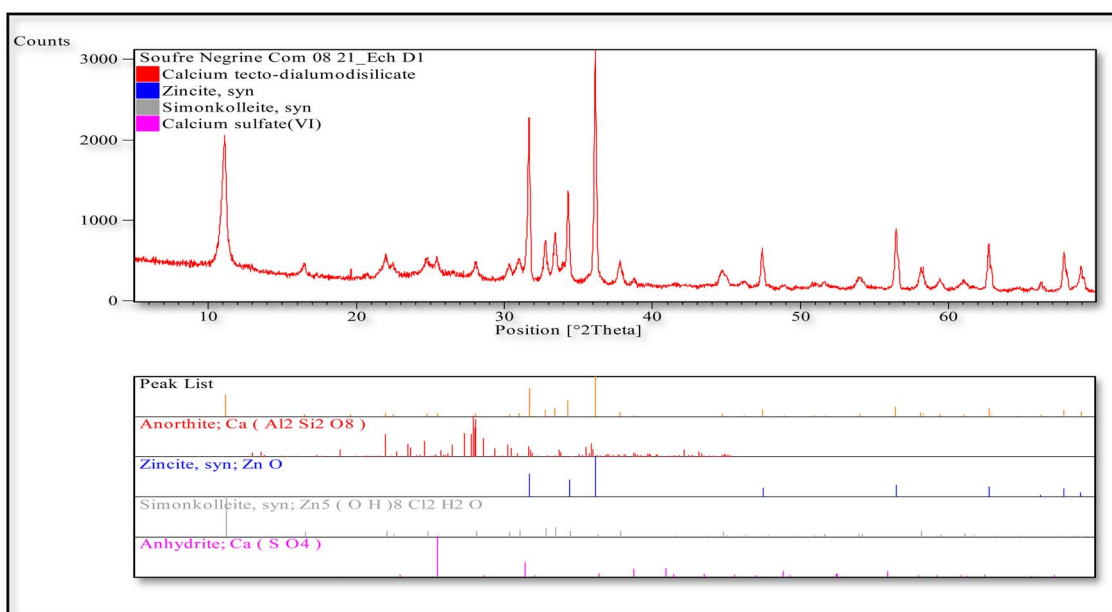

Fig. 5 XRD image of the SHAC of the adsorption of HCQ.

contribute to the observed decline in adsorption efficiency under these conditions.

3.2.2 Effect of the dose of SHAC. The amount of adsorbent is a key parameter that can significantly influence the efficiency of the adsorption process. To investigate its effect, equilibrium experiments were carried out under the following conditions: natural pH, room temperature (25 °C), and an initial HCQ concentration of 10 mg L^{-1}.

The results shown in Fig. 7 indicate that increasing the adsorbent mass significantly enhances the adsorption efficiency. As the mass increases from 0.1 g to 0.25 g, the removal rate rises from 43.21% to 50.41%, reaching a maximum efficiency of 83.38% with 0.75 g of adsorbent. This improvement is attributed to the greater availability of active sites, which facilitates more effective interaction and binding of HCQ molecules present in the solution.[23,26]

3.2.3 Effect of pH. pH is an essential factor in adsorption processes, as it influences not only the surface charge and structure of the adsorbent but also the ionization state of the adsorbate and the nature of their interactions. In this study, experiments were conducted using an initial HCQ concentration of 10 mg L^{-1}, at room temperature, and with an activated carbon dosage of 0.5 g L^{-1}.

The results are shown in the figure Fig. 5 that the adsorption performance exhibited a strong dependence on pH, with the maximum removal efficiency (72.72%) achieved at pH 6. At pH 3, the removal efficiency decreased to 62.42%, while a significant decline was observed at pH 9, with only 40.16% of HCQ removed. These variations can be attributed to the surface charge properties of the SHAC and the speciation behavior of HCQ in aqueous solution.

The point of zero charge (pHpzc) of the activated carbon was determined to be 7.1, indicating that the surface is positively charged at pH < 7.1 and negatively charged at pH > 7.1. Without forgetting that HCQ possesses three pK_a values (4.0, 8.3, and 9.7), which govern its ionization state across the pH range. At pH 6, HCQ exists primarily in a neutral or partially protonated form, and the SHAC surface is still positively charged, leading to favorable interactions such as π–π stacking or hydrogen bonding, which enhance adsorption.[27,28] At highly acidic pH (pH 3), both HCQ and the SHAC surface are strongly protonated, which may induce electrostatic repulsion and reduce adsorption efficiency. Conversely, at alkaline pH (pH 9), HCQ is predominantly deprotonated (negatively charged), while the SHAC surface also carries a negative charge, resulting in electrostatic repulsion that significantly hinders adsorption (Fig. 8).

These findings indicate that pH 6 offers the most favorable conditions for HCQ adsorption onto activated carbon, due to an optimal balance of surface charge and HCQ speciation, which promotes effective interaction between adsorbate and adsorbent.[23,29,30]

3.2.4 Effect of temperature. The influence of temperature on the adsorption process was investigated using a thermostatic bath, which allowed precise control of the temperature at 25 °C, 35 °C, 45 °C, and 55 °C. The experiments were conducted by adding 0.5 g of activated carbon to 1 L of HCQ solution, under controlled conditions.

Fig. 9 demonstrates that adsorption efficiency increases significantly with temperature. At 25 °C, approximately 60% of HCQ is removed after 240 minutes, while at 55 °C, the efficiency surpasses 80%. This behavior indicates that the adsorption process is likely endothermic, meaning it is favored by heat.

The improved performance at higher temperatures can be explained by the enhanced mobility of HCQ molecules, which facilitates their diffusion to the adsorbent surface and interaction with active sites. The thermal energy likely helps overcome activation barriers, leading to a higher adsorption rate and overall efficiency (Fig. 10).

3.3 Isotherms of adsorption

Adsorption isotherms are essential tools for understanding the nature of interactions between adsorbent and adsorbate, as well
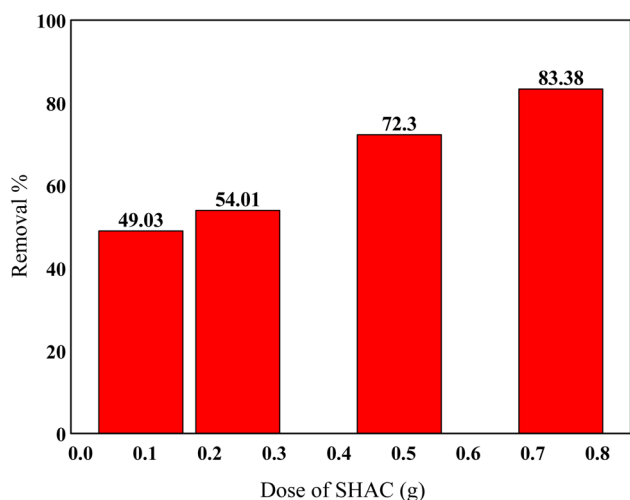

Fig. 7 Effect of the dose of SHAC onto the adsorption of HCQ (conditions: pH = 6, 10 mg L^{-1} of 25 °C of initial concentration and temperature).
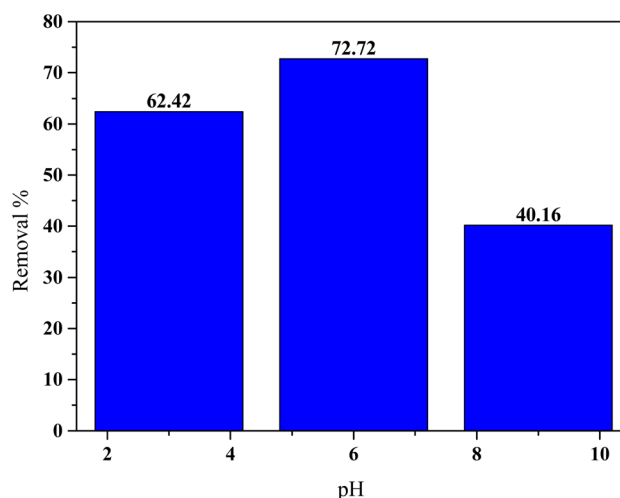

Fig. 8 Effect of pH onto the adsorption of HCQ (conditions: 10 mg L^{-1}, 25 °C of initial concentration and temperature).
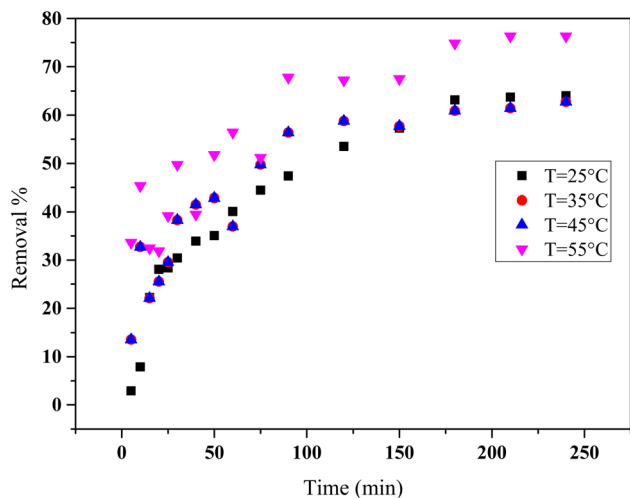
Fig. 9 Effect of temperature on HCQ removal efficiency over time (conditions: 10 mg L^{-1}, pH = 6 and SHAC dose = 0.5 g).

as for evaluating the adsorptive capacity of the material. In this study, we applied two of the most commonly used isotherm models, the Langmuir,[31] the Freundlich[32] and Temkin.[33] isotherms, to identify the one that best fits our experimental data.

$$q_e = \frac{q_{max} \times K_L \times C_e}{1 + K_L \times C_e} \qquad (6)$$

where q_e is the amount of solute adsorbed per unit mass of the adsorbent (capacity adsorption), K_L is the Langmuir constant, q_{max} is the maximum capacity adsorption. The K_L and q_{max} are deduced from the plot $1/q_e$ plotted *versus* $1/C_e$ (Fig. 11) and C_e is the concentration of the adsorbate in the bulk phase.

$$q_e = K_F C_e^{1/n} \qquad (7)$$

where q_e is the amount of solute adsorbed per unit mass of the adsorbent (capacity adsorption), K_F is the Freundlich constant

related to adsorption capacity, n is the Freundlich constant related to adsorption intensity. The K_F and n are deduced from the plot $\ln q_e$ plotted *versus* $\ln C_e$ (Fig. 12).

$$q_e = \frac{RT}{b} \ln K_T C_e \qquad (8)$$

The linearized form is:

$$q_e = B \ln K_T + B \ln C_e \qquad (9)$$

where $B = RT/b$, T is the absolute temperature. The fitted Temkin constants, b (kJ mol^{-1}) and K_T (L g^{-1}), denote heat of adsorption and maximum binding energy, respectively. The Temkin constant obtained from the plot q_e plotted *versus* $\ln C_e$ (Fig. 13).

The adsorption isotherms of HCQ onto SHAC from aqueous solutions are shown in Fig. 10. According to the Giles classification, the obtained curves exhibit an L-type isotherm, which indicates a strong affinity between HCQ molecules and the SHAC surface.[34] This type of isotherm suggests that adsorption sites are rapidly saturated, even at low solute concentrations, highlighting the high effectiveness of SHAC in binding HCQ.

Based on the results presented in Table 2, the Langmuir isotherm model provides a good fit for the adsorption process, with a maximum adsorption capacity (q_{max}) of 23.25 mg g^{-1}, indicating that the activated carbon can retain a substantial amount of the pollutant. The Langmuir constant (K_L) is 0.48 L mg^{-1}, suggesting a moderate affinity between the adsorbent and the adsorbate. Additionally, the correlation coefficient ($R^2 = 0.989$) confirms a strong agreement between the experimental data and the Langmuir model.

The Freundlich model also shows favorable adsorption characteristics, with a K_F value of 10.1 and an adsorption intensity (n) of 3.8, suggesting favorable multilayer adsorption. However, the lower R^2 value (0.87) indicates a weaker correlation with the experimental results compared to the Langmuir
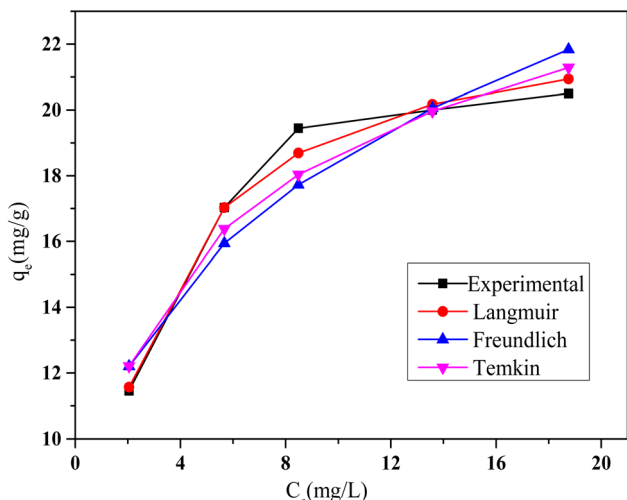

Fig. 10 Kinetic plots of non-linear equilibrium isotherm for the removal of HCQ by SHAC (conditions; pH 6, 0.5 g L^{-1} of adsorbent dose, 400 rpm of stirring speed, and temperature of 25 °C).
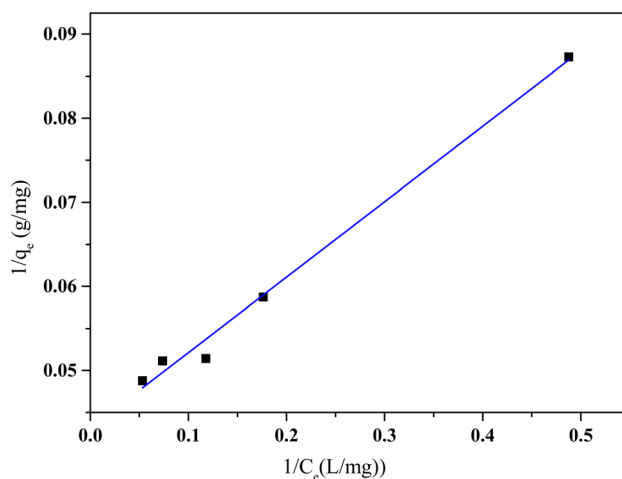

Fig. 11 Langmuir isotherm model of HCQ onto SHAC (conditions; pH 6, 0.5 g L^{-1} of adsorbent dose, 400 rpm of stirring speed, and temperature of 25 °C).
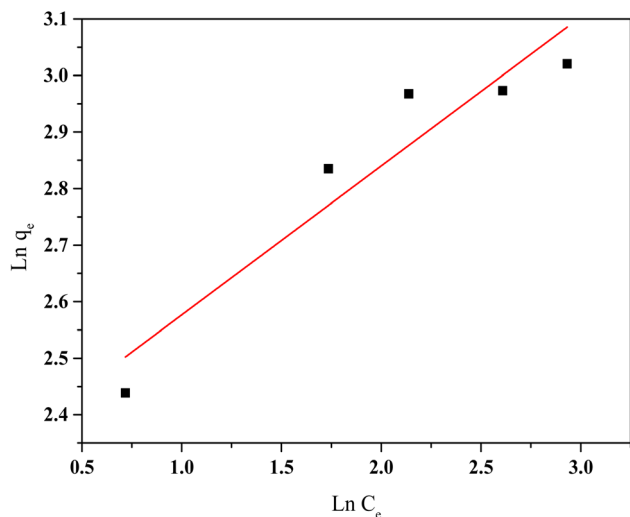
Fig. 12 Freundlich isotherm model of HCQ onto SHAC (conditions; pH 6, 0.5 g L^{-1} of adsorbent dose, 400 rpm of stirring speed, and temperature of 25 °C).
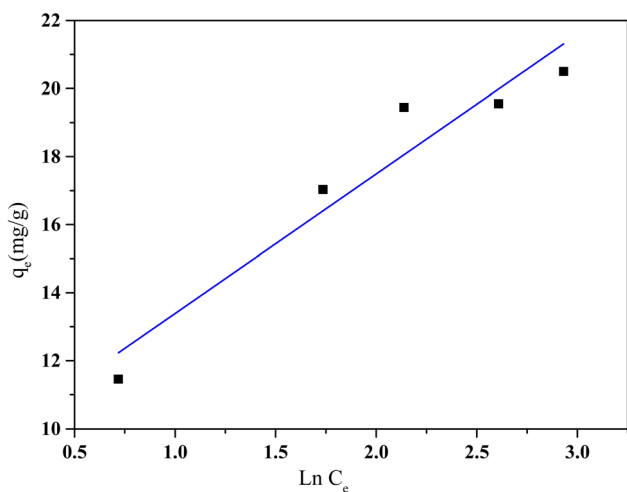

Fig. 13 Temkin isotherm model of HCQ onto SHAC (conditions; pH 6, 0.5 g L^{-1} of adsorbent dose, 400 rpm of stirring speed, and temperature of 25 °C).

Table 2 Physical properties of SHAC

	Value	Units
S_{BET}	258.13	m^2 g^{-1}
V_{Total}	0.202	cm^3 g^{-1}
Average pore diameter	37	Å

model. Overall, the findings show that monolayer adsorption on a homogeneous surface, as described by Langmuir, is more consistent with the observed behavior.

The Temkin isotherm model also provided a reasonable fit to the experimental data, with a correlation coefficient (R^2) of 0.90. The positive K_T value, which are associated with the heat of

sorption, indicate the presence of weak interactions between the sorbent and the sorbate.

3.4 Adsorption kinetic modelling

The kinetic study of hydroxychloroquine (HCQ) adsorption onto SHAC was carried out to better understand the mechanisms involved in the adsorption process. Two kinetic models were applied: the pseudo-second-order model[35,36] and the intra-particle diffusion model.[37,38] The pseudo-second-order model helps evaluate whether the adsorption process is governed by chemical interactions between the activated carbon and HCQ molecules, suggesting chemisorption. The intraparticle diffusion model, on the other hand, is used to determine whether the adsorption rate is limited by the diffusion of HCQ molecules into the pores of the activated carbon. Analyzing the experimental data using these two models will allow us to identify the dominant mechanism, assess the adsorption capacity of the material, and optimize the operating conditions for effective removal of HCQ from aqueous solutions.

The pseudo-first-order kinetic model was excluded from this study due to its poor agreement with the experimental adsorption data.

The results, calculated using eqn (10) and (11), are summarized in Table 3.

$$\frac{t}{q_t} = \frac{1}{K_2 \times q_e^2} + \frac{t}{q_e} \tag{10}$$

$$q_e = k_{id} \times t^{0.5} + C \tag{11}$$

where q_e and q_t (mg g^{-1}) represent the amount of dye adsorbed at equilibrium and at time t (min), respectively. k_2 (g mg^{-1} min^{-1}) and k_{id} (mg g^{-1} min$^{-1/2}$) denote the adsorption rate constants for pseudo-second order and the intra-particle diffusion rate constant.

The plots of t/q_t *versus* time (Fig. 14) show a strong linear correlation across all tested initial concentrations, suggesting that the pseudo-second-order kinetic model provides an excellent fit for the adsorption data. This is further supported by high R^2 values (above 0.96), indicating a strong agreement between the model and the experimental results. Moreover, the theoretical qe values derived from the model are consistent with the experimental values, confirming the reliability of this model in describing the adsorption kinetics. These findings point to a chemically controlled process, likely involving strong adsorbate–adsorbent interactions.

Additionally, the q_t *versus* $t^{0.5}$ plots (Fig. 15), constructed for varying initial concentrations of HCQ, revealed a multi-linear behavior, indicative of a multi-step adsorption process. The

Table 3 Isotherm parameters for the adsorption of HQC on SHAC

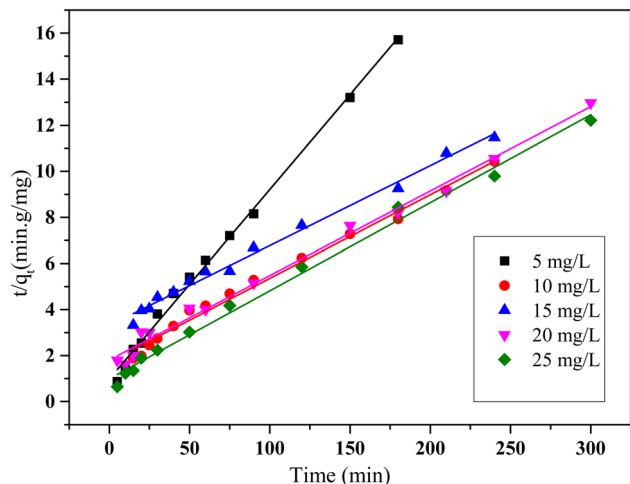|	Langmuir			Freundlich			Temkin		
Adsorbent	R^2	q_m	K_L	R^2	n	K_F	R^2	B_T	K_T
SHAC	0.989	23.25	0.48	0.87	3.84	10.10	0.90	4.10	9.58

Fig. 14 Kinetic plot of pseudo-second order model for HCQ onto SHAC (conditions; pH 6, 0.5 g L^{-1} of adsorbent dose, 400 rpm of stirring speed, and temperature of 25 °C).

initial steep region corresponds to external surface diffusion, characterized by rapid transport of molecules to the adsorbent surface. This is followed by a gentler slope, representing intra-particle diffusion into the porous structure of the activated carbon. The final plateau reflects the establishment of adsorp-tion equilibrium.

Since none of the lines intersect the origin, it can be inferred that intraparticle diffusion is not the only rate-limiting step. Instead, the process involves a combination of film diffusion and pore diffusion, underscoring the complexity of the adsorption mechanism.

3.5 Thermodynamic parameters

Thermodynamic parameters, such as Gibbs free energy (ΔG), enthalpy (ΔH), and entropy (ΔS), provide important information

on the feasibility and mechanism of adsorption processes. Adsorption is always associated with a thermal effect, which may be exothermic ($\Delta H < 0$) or endothermic ($\Delta H > 0$). Depending on the nature of the interaction.

Among these parameters, ΔH is particularly informative, as it helps differentiate between physisorption and chemisorption, offering insights into the interaction mechanisms between the adsorbent and the adsorbate (Table 4).

These parameters are typically evaluated using the van't Hoff equation, as shown below:

$$\ln K_{\mathrm{d}} = -\frac{\Delta H^{\circ}}{RT} + \frac{\Delta S^{\circ}}{T} \tag{12}$$

$$K_{\mathrm{d}} = \frac{q_{\mathrm{e}}}{C_{\mathrm{e}}} \tag{13}$$

$$\Delta G^{\circ} = \Delta H^{\circ} - T\Delta S^{\circ} \tag{14}$$

where K_{d} is the distribution constant (L g^{-1}), R is the universal gas constant (8.314 J mol K^{-1}) and T is the solution temperature in K. The enthalpy (ΔH°) and entropy (ΔS°) were estimated from the slope and intercept of the plot ln K_{d} versus $1/T$, respectively (Fig. 16).

Table 5 presents the thermodynamic parameters ΔH°, ΔS°, and ΔG° along with the coefficient of determination (R^2), derived from the van't Hoff plot of ln K_{d} versus $1/T$. The positive ΔH° values indicate that HCQ adsorption onto SHAC is endo-thermic, requiring energy input, while the positive ΔS° values reflect increased disorder at the solid–liquid interface, likely due to the displacement of water molecules from the adsorbent surface. The negative ΔG° values confirm that the adsorption process is spontaneous and thermodynamically favorable. Notably, the trend of ΔG° becoming less negative with rising temperature suggests a slight decrease in spontaneity at higher temperatures, indicating that, despite its endothermic nature, increasing temperature does not significantly enhance adsorp-tion under the studied conditions.

4 Adsorption mechanisms

The adsorption mechanism of hydroxychloroquine sulfate onto involves a combination of porosity-driven physisorption and specific surface interactions. The activated carbon exhibits a high specific surface area (258.13 m^2 g^{-1}), and predominantly mesoporous structure, which facilitates the diffusion and accessibility of hydroxychloroquine molecules into the porous network, consistent with known structure-adsorption relation-ships for organic micropollutants on mesoporous carbons.[39,40] The point of zero charge (pH$_{\mathrm{pzc}}$ = 7.1) of the carbon surface indicates that at solution pH values above this point the surface becomes increasingly negatively charged, enhancing electro-static attractions with protonated forms of hydroxychloroquine, a mechanism frequently invoked for basic pharmaceutical compounds in aqueous adsorption studies.[41,42]

In addition, hydrogen bonding interactions between surface oxygen-containing functional groups (–OH, –COOH) enriched during ZnCl$_2$ activation and the amine or hydroxyl moieties of
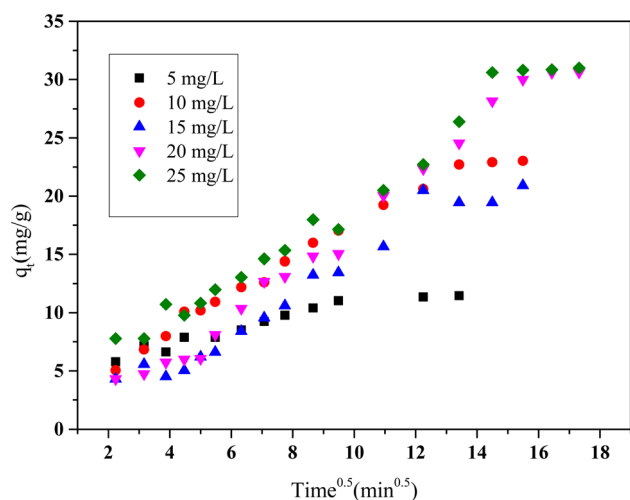

Fig. 15 Kinetic plot of intraparticle diffusion model for HCQ onto SHAC (conditions; pH 6, 0.5 g L^{-1} of adsorbent dose, 400 rpm of stirring speed, and temperature of 25 °C).

Table 4 Kinetic parameters for the adsorption of HCQ onto SHAC

Pseudo-second-ordre				Intraparticule diffusion	
[C] (mg L^{-1})	R^2	q_e (mg g^{-1})	k_2 (g mg^{-1} min)	R^2	K_i (mg g^{-1} $min^{0.5}$)
5	0.995	12.19	0.0069	0.913	0.526
10	0.988	27.54	0.00076	0.981	1.409
15	0.99	28.81	0.00036	0.960	1.439
20	0.991	27.77	0.00072	0.987	1.982
25	0.992	26.31	0.0014	0.970	1.728
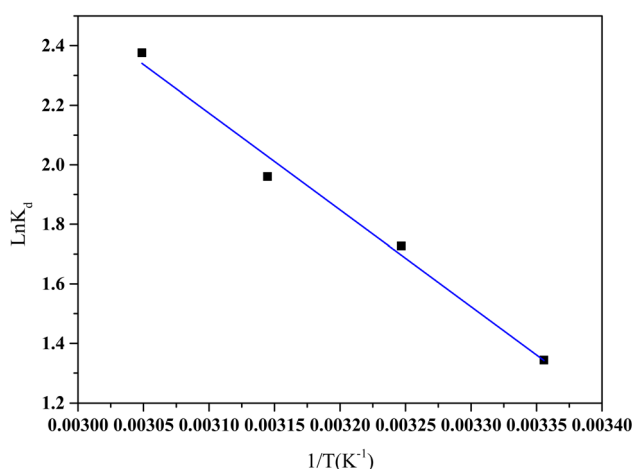
Fig. 16 The plot of the K_d vs. $1/T$ for the HCQ adsorption onto SHAC (conditions; pH 6, 10 mg L^{-1} HCQ concentration, 0.5 g L^{-1} of adsorbent dose and 400 rpm of stirring speed).

Table 5 Thermodynamic parameters for the adsorption of HCQ drug onto SHAC

T (°C)	$\Delta G°$ (kJ mol^{-1})	$\Delta H°$ (kJ mol^{-1})	$\Delta S°$ (kJ mol^{-1})	R^2
298	−3.32	27.04	0.1019	0.981
308	−4.34			
318	−5.00			
328	−6.38			

Table 6 Comparison of the adsorption capacities of different adsorbents for the removal of HCQ

Adsorbents	Adsorption capacities	Reference
Cocoa shell AC	14.64 mg g^{-1}	23
Koalin	66.22 mg g^{-1}	29
Zeolith cliniptilolit	6.38 mg g^{-1}	30
Carboxylated lignin spong	0,165 mmol g^{-1}	41
Composite ($MgZnAl(CO_3^{2-})$	84.40 mg g^{-1}	44
Algal biodiesel biochar	353,5 µg g^{-1}	45
SHAC	23.17 mg g^{-1}	This study

hydroxychloroquine contribute to adsorption, as demonstrated for other pharmaceutical adsorbates on carbonaceous matrices.[42] Complementarily, π–π electron interactions between the aromatic of hydroxychloroquine and the graphitic domains of the activated carbon further stabilize adsorption, a phenomenon widely reported in activated carbon systems for organic compound uptake.[43]

Collectively, these mechanisms suggest that hydroxychloroquine adsorption is dominated by physisorption within mesopores, facilitated by surface chemistry and electrostatic/hydrogen bonding interactions, which is in agreement with mechanistic frameworks proposed for similar pharmaceutical pollutant adsorption on mesoporous carbons.[41]

5 Comparative study

A comparative study of various adsorbents for HCQ removal revealed significant differences in adsorption capacities, primarily due to variations in surface area, pore structure, and functional groups on the adsorbent surfaces. Modified and composite adsorbents generally show higher capacities, indicating stronger interactions with HCQ molecules. As shown in Table 6, our activated carbon demonstrates excellent HCQ removal efficiency and is also environmentally friendly.

6 Conclusion

This study presents an environmentally friendly and cost-effective adsorbent for the removal of recalcitrant pharmaceuticals, such as hydroxychloroquine (HCQ), *via* adsorption. Activated carbon was synthesized from *Scolymus hispanicus*, an agricultural waste. BET, SEM, and XRD analyses indicated that the resulting SHAC exhibits a high surface area (258.13 m^2 g^{-1}) and mesoporous structure, promoting efficient adsorption of HCQ molecules. This approach offers a sustainable solution for reducing pharmaceutical contaminants in water, contributing to environmental protection.

The experimental results demonstrated that acidic conditions (pH 3.5) significantly enhanced adsorption, achieving a maximum removal efficiency of 83.45%. Increasing the adsorbent dose to 0.75 g improved performance to 83.38%, whereas higher initial HCQ concentrations (25 mg L^{-1}) reduced efficiency to below 30%, likely due to site saturation. Elevated temperatures also improved adsorption, with efficiencies exceeding 80% at 55 °C, confirming the endothermic nature of the process.

Among the tested isotherm models, the Langmuir model provided the best fit, indicating monolayer adsorption and

yielding a maximum capacity of 23.15 mg g^{-1}. Kinetic studies revealed that the pseudo-second-order model best described the adsorption process, suggesting that chemical interactions play a significant role. Thermodynamic analysis further supported this, showing negative $\Delta G°$ values, along with positive $\Delta H°$ and $\Delta S°$, confirming a spontaneous, favorable, and endothermic adsorption mechanism.

In conclusion, *Scolymus hispanicus*-based activated carbon exhibits strong potential as a low-cost, bio-based, and environmentally friendly adsorbent for HCQ removal, offering a viable solution for advanced water treatment applications.

Author contributions

A. Hamadi: methodology, data analysis, original draft preparation, writing review and editing, I. Hammoudi, F. Finnouche and H. Kais: provision of materials and manuscript review, N. Yeddou-Mezenner: investigation, visualization, Z. Nekkaa: validation resources. All authors have read and approved the final version of the manuscript.

Conflicts of interest

The authors declare no competing interests.

Data availability

All data supporting the results of this study are provided within the article. Additional information may be obtained from the corresponding author upon reasonable request.

Supplementary information (SI): further results on the removal of the HCQ drug, the valorization of Scolymus hispanicus as activated carbon, as well as comprehensive characterization analyses, experimental procedures, and detailed kinetic and thermodynamic studies presented in this manuscript. See DOI: https://doi.org/10.1039/d5ra08507a.

References

1 T. A. der Beek, F. A. Weber, A. Bergmann, S. Hickmann, I. Ebert, A. Hein and A. Küster, *Environ. Toxicol. Chem.*, 2016, **35**(4), 823–835.

2 P. Verlicchi, M. Al Aukidy and E. Zambello, *Sci. Total Environ.*, 2012, **429**, 123–155.

3 R. Maa, B. Wanga, L. Yina, Y. Zhanga, S. Denga, J. Huanga, Y. Wanga and G. Yua, *J. Hazard. Mater.*, 2017, **323**, 147–155, DOI: 10.1016/j.jhazmat.2016.05.030.

4 C. L. Bell, *Am. J. Med.*, 1983, **75**, 46–51, DOI: 10.1016/0002-9343(83)91270-6.

5 T. Dörner, *Nat. Rev. Rheumatol.*, 2010, **6**, 10–11, DOI: 10.1038/nrrheum.2009.235.

6 R. I. Rynes, *Am. J. Med.*, 1988, **85**, 18–22, DOI: 10.1016/0002-9343(88)90357-9.

7 L. Tanenbaum and D. L. Tuffanelli, *Arch. Dermatol.*, 1980, **116**, 587–591, DOI: 10.1001/archderm.1980.01640290097026.

8 I. B. Zvi, S. Kivity, P. Largevity and Y. Shoenfeld, *Clin. Rev. Allergy Immunol.*, 2012, **42**, 145–153, DOI: 10.1007/s12016-010-8243-x.

9 S. Dong, L. Cui, Y. Tian, L. Xia, Y. Wu, J. Yu, D. M. Bagley, J. Sun and M. Fan, *J. Hazard. Mater.*, 2020, **399**, 123017, DOI: 10.1016/j.jhazmat.2020.123017.

10 K. Fent, A. A. Weston and D. Caminada, *Aquat. Toxicol.*, 2006, **76**(2), 122–159.

11 S. I. Al-Saeedi, M. Ashour and A. E. Alprol, *Front. Mar. Sci.*, 2023, **10**, 1202362, DOI: 10.3389/fmars.2023.1202362.

12 S. Kainth, P. Sharma and O. P. Pandey, *Appl. Surf. Sci. Adv.*, 2024, **19**, 100562, DOI: 10.1016/j.apsadv.2023.100562.

13 Y. N. Zhang, *et al.*, *Desalin. Water Treat.*, 2018, **123**, 227–287, DOI: 10.5004/dwt.2018.22778.

14 Y. Xin Yu, *J. Colloid Interface Sci.*, 2025, **695**, 137799, DOI: 10.1016/j.jcis.2025.137799.

15 W. Al-Gethami, M. A. Qamar, M. Shariq, A.-N. M. A. Alaghaz, A. Farhan, A. A. Areshi and M. H. Alnasir, *RSC Adv.*, 2024, **14**, 2804–2834, DOI: 10.1039/D3RA06501D.

16 R. H. Perry, *Phys. Chem. Chem. Phys.*, 2021, **23**, 1221–1233, DOI: 10.1039/D0CP05543C.

17 B. Barkahoum, *et al*, *RSC Adv.*, 2025, **15**, 3066–3079, DOI: 10.1039/d4ra07917e.

18 Md. Aminul Islam, M. K. Nazal, M. Sajid and M. Altahir Suliman, *J. Mol. Liq.*, 2024, **396**, 123976, DOI: 10.1016/j.molliq.2024.123976.

19 G. Crini and E. Lichtfouse, *Environ. Chem. Lett.*, 2019, **17**, 145–155.

20 O. A. Timothy, O. O. Peter and O. O. Elizabeth, *Kuwait J. Sci.*, 2024, **51**(3), 100225, DOI: 10.1016/j.kjs.2024.100225.

21 M. Kobya, *et al*, *Bioresour. Technol.*, 2005, **96**, 1518–1521, DOI: 10.1016/j.biortech.2004.12.005.

22 D. A. Rodríquez-Alejandro, *et al.*, *Energy Convers. Manage.*, 2023, **288**, 117114, DOI: 10.1016/j.enconman.2023.117114.

23 F. Finnouche, A. Hamadi, H. Kais, N. Yeddou and Z. Nekkaa, *J. Dispersion Sci. Technol.*, 2024, **83**, 1–84, DOI: 10.1080/01932691.2024.2302069.

24 L. S. Čerović, S. K. Milonjić, M. B. Todorović, M. I. Trtanj, Y. S. Pogozhev, Y. Blagoveschenskii and E. A. Levashov, *Colloids Surf., A*, 2007, **297**, 1–6, DOI: 10.1016/j.colsurfa.2006.10.0.

25 K. S. Sing, *Pure Appl. Chem.*, 1985, **57**, 603–619.

26 J. O. Amode, J. H. Santos, Z. M. Alan, A. H. Miraz and C. C. Mei, *Int. J. Ind. Chem.*, 2016, **7**(3), 333–345, DOI: 10.1007/s40090-016-0085-9.

27 T. Acar, M. B. Arvas, B. Ucar and Y. Sahin, *Adsorption*, 2024, **30**, 1377–1393, DOI: 10.1007/s10450-024-00506-2.

28 A. F. M. Streit, G. Collezza, S. P. Druzian, R. S. Verdi and E. L. Felleto, *Chemosphere*, 2021, **262**, 128322, DOI: 10.1016/j.chemosphere.2020.128322.

29 H. Bendjeffal, M. Ziati, A. Aloui, H. Mamine, T. Metidji, A. Djebli and Y. Bouhedjaet, *Int. J. Environ. Anal. Chem.*, 2021, **103**, 1982–2003, DOI: 10.1080/03067319.2021.1887162.

30 P. N. Ramiro, D. M. Paula and A. M. Luiza Carla, NOS. Mara Heloisa, *Water, Air, Soil Pollut.*, 2022, **233**, 287, DOI: 10.1007/s11270-022-05787-3.

31 I. Langmuir, *J. Am. Chem. Soc.*, 1918, **40**, 1361–1403, DOI: 10.1021/ja02242a004.

32 H. Z. Freundlich, *J. Phys. Chem.*, 1906, **57**, 385–471.

33 D. M. Araujo, *et al.*, *Appl. Sci.*, 2022, **12**, 699, DOI: 10.3390/app12020699.

34 C. H. Giles, *J. Chem. Soc.*, 1960, **111**, 3973, DOI: 10.1039/jr9600003973.

35 N. Bensalah, S. Midassi, M. I. Ahmad and A. Bedoui, *Chem. Eng. J.*, 2020, **402**, 126279, DOI: 10.1016/j.cej.2020.126279.

36 C. López-Otín, M. A. Blasco, L. Partridgr, M. Serrano and G. Kroemer, *Cell*, 2023, **186**, 243–278, DOI: 10.1016/j.cell.2022.11.001.

37 M. Abbas, A. Zaini, Y. Amano and M. Machida, *J. Hazard. Mater.*, 2009, **180**, 552–560, DOI: 10.1016/j.jhazmat.2010.04.069.

38 S. Zhang, K. Hyde, J. Liu and M. Abdel-Wahad, *Phytotaxa*, 2019, **408**, 195–207, DOI: 10.11646/phytotaxa.408.3.4.

39 R. Ghorbali, L. Sellaoui, H. Ghalla, A. Bonilla-Petriciolet, R. Trejo-Valencia, A. Sánchez-Barroso, S. Deng and A. B. Lamine, *Environ. Sci. Pollut. Res.*, 2024, **31**, 39208–39216, DOI: 10.1007/s11356-024-33806-9.

40 T. Hubetska, N. Kobylinska and J. R. García, *Adsorption*, 2020, **26**, 251–266, DOI: 10.1007/s10450-019-00143-0.

41 B. Gao, H. Liang, J. Wang, Y. Huang, J. Wang, J. Song, P. Hu, H. Yang and S. Ma, *Sep. Purif. Technol.*, 2025, **354**, 129359, DOI: 10.1016/j.seppur.2024.129359.

42 H. N. Tran, Y. F. Wang, S. J. You and H. P. Chao, *Process Saf. Environ. Prot.*, 2017, **107**, 168–180, DOI: 10.1016/j.psep.2017.02.010.

43 N. Samghouli, I. Bencheikh, K. Azoulay, S. Jansson and S. El Hajjaji, *Environ. Monit. Assess.*, 2025, **197**, 259, DOI: 10.1007/s10661-025-13685-4.

44 Y. Rachid, *et al.*, *J. Environ. Chem. Eng.*, 2025, 13–118483, DOI: 10.1016/j.jece.2025.118438.

45 D. Gümüş and F. Gümüş, *Arabian J. Sci. Eng.*, 2021, **47**(6), 7325–7334, DOI: 10.1007/s13369-021-06235-w.